*Institute of Space and Aeronautical Science, University of Tokyo*
*Report No. 521, January 1975*

# Dynamic Behavior of Viscoelastic Shallow Spherical Shells

By

Megumi SUNAKAWA and Nori KUMAI

*Summary*: On the basis of nonlinear theory, the axisymmetric dynamic behavior of viscoelastic shallow spherical shells is analyzed. Two types of loading condition, that is, step and graded loadings, are considered and a linear model is used to describe the viscoelastic characteristics of materials. The governing equations derived by the authors are solved numerically, and the critical load and the effects of viscoelasticity and loading speed on the dynamic behavior are discussed. It is pointed out that buckling phenomena must be analyzed paying attention to the role of time, since dynamic, static and creep bucklings are related with one another as a function of time. And a clear definition of dynamic buckling is proposed. The theoretical predictions show a good agreement with experimental results. From the present results, the quasi-static buckling load is also obtained immediately. The dynamic behavior of elastic shells obtained by the present procedure coincides excellently with those reported so far.

## 1. INTRODUCTION

Light-weight structures, especially thin plate and shell structures, have high specific load-carrying capabilities. However, they are subject to large deformations accompanied with unstable phenomena when loads exceed a critical level. That is, although loads proportional to their own weight are decreased, the reduction of structural weight, in general, results in decreases in the strength and stiffness of structures when the forms of the structures and materials used remain the same. Pertinent evaluation of environmental conditions (loads) and a clear estimation of the resulting responses of structures and structural components are very important in determining structural forms and materials and therefore in establishing the reliability of structures.

Shells are one of the main types of structural members of surface and underwater structures and vehicles as well as of aircraft, rockets and spacecraft. And so it is important to investigate the stability characteristics of shell structures under various environmental conditions. The most important of instability phenomena is buckling.

Research on problems of buckling has been carried out for a long time, but it is nevertheless very difficult to obtain definite solutions, especially when the wide variations in the forms of structures, material properties and environmental conditions have to be taken into consideration.



This document is provided by JAXA.

The behavior and stability of shell structures subjected to dynamic and impulsive loadings are not only very interesting problems in themselves but are also of practical importance. These problems, however, have not yet been satisfactorily analyzed as compared with the corresponding static ones.

The behavior of dynamic snap-through of spherical shells has been investigated by several authors. Humphreys and Bodner (1962), using the Rayleigh-Ritz method, have studied the axisymmetric behavior of elastic clamped spherical shells under uniformly distributed impulsive loads; Budiansky and Roth (1962), using the Galerkin method, have obtained an approximate solution for the similar problem, and Simitses (1967) has used a modified Ritz-Galerkin procedure and found the minimum possible critical impulse for snap-through. Archer and Lange (1965) and Huang (1969) have obtained the exact solution of fundamental equations for dynamic buckling problem, using a direct numerical method. In the research mentioned above, it has been assumed that the deformation is axisymmetric. Liepins (1969) has obtained a direct numerical solution for the problem of asymmetric dynamic response and buckling of elastic shallow spherical shells. For the details of research carried out so far, see Reference [*16*].

In the present paper, the axisymmetric nonlinear dynamic behavior of viscoelastic thin shallow spherical shells with a clamped edge subjected to uniformly distributed step and graded loadings is studied, where a linear model is used to describe the viscoelastic characteristics of materials.

The present research will analyze the effects of viscoelasticity and loading speed on the dynamic behavior and buckling load, and the relationship between the applied load and time until large deformation (buckling) occurs. By studying the variation of buckling load with loading speed, the connection between dynamic and static bucklings is examined. Relationships among dynamic, static and creep (static buckling accompanied with creep deformation) bucklings are also investigated, paying attention to the fact that they are related with one another as a function of time. At the same time, a clear definition of dynamic buckling is proposed.

In order to observe the response of viscoelastic spherical shells to dynamic loading and to check the results of the numerical solution, some experiments have been carried out and a good agreement between the theoretical predictions and experimental results is seen.

The quasi-static buckling load and the behavior of elastic shells are also shown.

The present work forms a link in the chain of the authors' research which intends to make the mechanism of snap-through phenomena in shells clear.

## Nomenclature

| | |
|---|---|
| $a$ | base radius. |
| $B$ | viscoelastic constant, $B \equiv (E/E_1)\tau_2(E/m)^{1/2}/R$. |
| $\beta, \theta$ | polar and circumferential angles, respectively. |
| $\beta_0$ | angle of the semi-apex of the shell. |

This document is provided by JAXA.

$E$ constant which has a dimension of stress.
$E_0$ static Young's modulus, $E_0 \equiv 1/[1/E_1 + 1/E_2]$.
$E_1, E_2$ Young's moduli. (Fig. 2)
$\varepsilon$ strain component.
$\eta_2$ coefficient of viscosity.
$f, F$ nondimensional and dimensional stress functions, respectively.
$h$ thickness of the shell.
$H$ rise of the middle surface at the center.
$J, I$ Bessel function of the first kind and the modified Bessel function of the first kind, respectively.
$\kappa$ change of curvature.
$\lambda$ shell parameter, $\lambda \equiv 2[3(1-\nu^2)]^{1/4}(H/h)^{1/2}$.
$m$ mass per unit volume.
$M$ bending moment.
$\nu$ Poisson's ratio.
$p$ nondimensional pressure load, $p \equiv q/q_0$.
$p_c$ nondimensional dynamic buckling load.
$p_{s0}$ nondimensional static buckling load of elastic shells (Young's modulus: $E_0$) and of viscoelastic shells.
$p_{s1}$ nondimensional static buckling load of elastic shells (Young's modulus: $E_1$).
$q$ pressure load.
$q_0$ classical buckling load, $q_0 \equiv \{2E/[3(1-\nu^2)]^{1/2}\}(h/R)^2$.
$Q_r$ transverse shearing force.
$R$ radius of curvature of the shell.
$\rho$ mean deformation, $\rho = \left[\iint WR^2 \sin\beta \, d\beta d\theta\right] \Big/ \left[\iint z_0 R^2 \sin\beta \cos\beta \, d\beta d\theta\right]$, where $z_0 = H(1-\xi^2)$.
$\sigma$ stress component.
$t, \tau$ time and nondimensional time, respectively.
$t^*, \tau^*$ time and nondimensional time until the load becomes constant, respectively. (Fig. 3)
$\tau_2$ retardation time, $\tau_2 \equiv \eta_2/E_2$.
$U, W$ meridional and normal displacements, respectively.
$w$ nondimensional normal displacement.
$w_n$ eigenmode of clamped circular plates.
$\xi$ nondimensional coordinate, $\xi \equiv (R/a)\beta$.
$\Phi, \Psi$ operators defined by Eqs. (2.2) and (3.16).
$\Phi_0$ operator, $\Phi_0 \equiv \Phi E$.

Bar over letter refers to the middle surface.
Subscripts $r$ and $\theta$ indicate the meridional and circumferential directions, respectively.

This document is provided by JAXA.

## 2. Governing Equations

A viscoelastic spherical shell as shown in Fig. 1 is considered, and it is assumed that the shell is subjected to external dynamic pressure.

In the present analysis, the following assumptions are introduced.

(1) the spherical shell is shallow, that is, the semi-apex angle of the shell is small,
(2) the shell is perfect, that is, any imperfection is not considered,
(3) the environmental conditions, such as thermal conditions, etc., are constant,
(4) the deformation pattern is axisymmetrical,
(5) inertia terms except $\partial^2 W/\partial t^2$ can be neglected,
(6) the characteristics of viscoelastic materials can be described by a linear model, and
(7) Poisson's ratio of materials is independent of time [3], [18].

For a linear viscoelastic model, the constitutive equatoin is given by

$$\Phi\sigma = \Psi\varepsilon, \tag{2.1}$$

where

$$\Phi = \sum_{m=0}^{N} \varphi_m(\partial/\partial t)^m, \qquad \Psi = \sum_{m=0}^{M} \psi_m(\partial/\partial t)^m. \tag{2.2}$$

According to assumption (7), the constitutive equation in the two-dimensional problem is written as

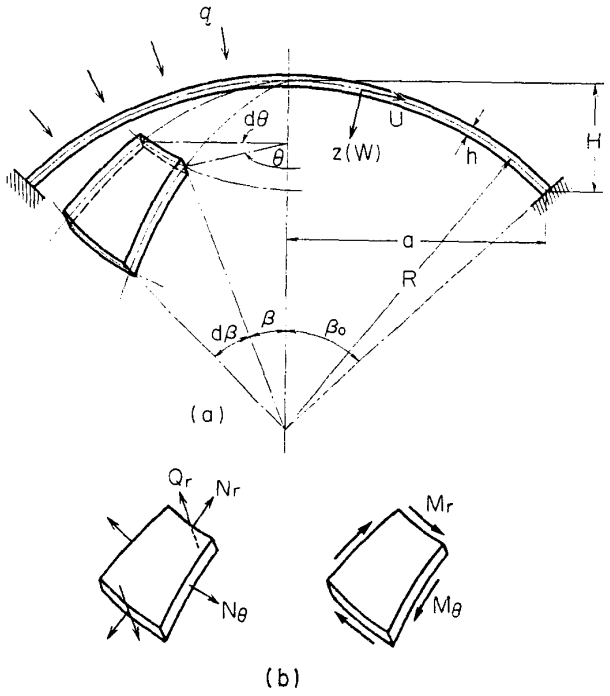


Fig. 1. Partial spherical shell.
(a) Shell geometry.
(b) Stress resultants and moments.

This document is provided by JAXA.

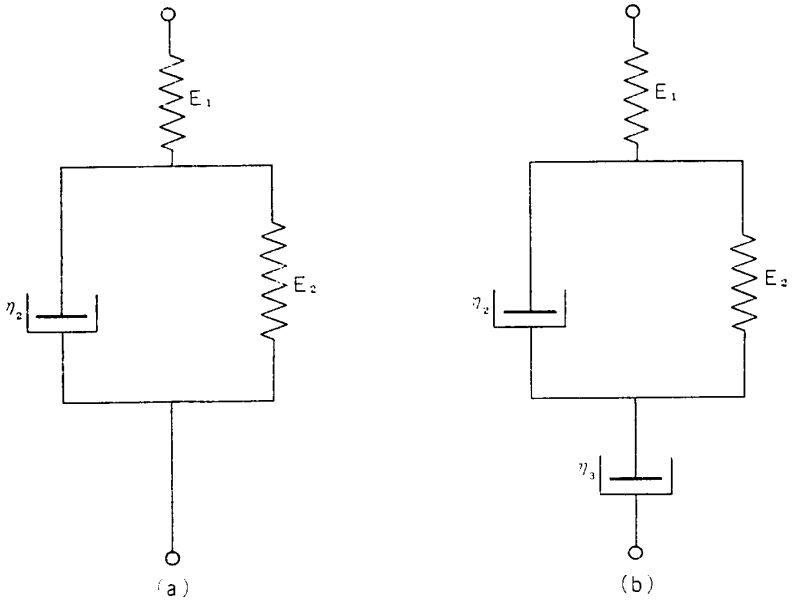


FIG. 2. Linear viscoelastic models.

$$\left.\begin{aligned} \Phi\sigma_r &= \Psi(\varepsilon_r + \nu\varepsilon_\theta)/(1-\nu^2), \\ \Phi\sigma_\theta &= \Psi(\varepsilon_\theta + \nu\varepsilon_r)/(1-\nu^2), \end{aligned}\right\} \quad (2.3)$$

where, $\sigma_r$ and $\sigma_\theta$ are meridional and circumferential stress components, respectively, and using the hypothesis of Kirchhoff-Love, strain components can be given as follows,

$$\left.\begin{aligned} \varepsilon_r &= \bar{\varepsilon}_r + z\kappa_r, \\ \varepsilon_\theta &= \bar{\varepsilon}_\theta + z\kappa_\theta. \end{aligned}\right\} \quad (2.4)$$

The strain components and change of curvatures of the middle surface for the case of axisymmetric deformation can be expressed as in Eqs. (2.5) and (2.6), where terms up to the second order of infinitesimal have been taken into consideration.

$$\left.\begin{aligned} \bar{\varepsilon}_r &= \frac{1}{R}\frac{\partial U}{\partial\beta} - \frac{W}{R} + \frac{1}{2R^2}\left(\frac{\partial W}{\partial\beta}\right)^2, \\ \bar{\varepsilon}_\theta &= \frac{U}{R}\cot\beta - \frac{W}{R}, \end{aligned}\right\} \quad (2.5)$$

$$\left.\begin{aligned} \kappa_r &= -\frac{1}{R^2}\frac{\partial^2 W}{\partial\beta^2}, \\ \kappa_\theta &= -\frac{1}{R^2}\frac{\partial W}{\partial\beta}\cot\beta. \end{aligned}\right\} \quad (2.6)$$

The equation of equilibrium in the $\beta$-direction and the equation of motion in the $z$-direction are expressed by Eqs. (2.7) and (2.8), respectively.

This document is provided by JAXA.

$$\frac{\partial \bar{\sigma}_r}{\partial \beta}+(\bar{\sigma}_r-\bar{\sigma}_\theta)\cot\beta=0, \tag{2.7}$$

$$\begin{aligned} h\Big[\bar{\sigma}_r R\sin\beta+\bar{\sigma}_r\frac{\partial^2 W}{\partial\beta^2}\sin\beta+\bar{\sigma}_\theta\Big(\frac{\partial W}{\partial\beta}+R\sin\beta\Big)\Big] \\ +R^2\Big(q-hm\frac{\partial^2 W}{\partial t^2}\Big)\sin\beta+R\sin\beta\Big(\frac{\partial Q_r}{\partial\beta}+Q_r\cot\beta\Big)=0, \end{aligned} \tag{2.8}$$

where $m$ is mass per unit volume.

The equation of equilibrium of bending moment is given by

$$RQ_r\sin\beta-M_r\cos\beta-\frac{\partial M_r}{\partial\beta}\sin\beta+M_\theta\cos\beta=0, \tag{2.9}$$

where

$$\left.\begin{aligned} \Phi M_r&=\int\Phi\sigma_r z dz=\frac{h^3\Psi}{12(1-\nu^2)}(\kappa_r+\nu\kappa_\theta), \\ \Phi M_\theta&=\int\Phi\sigma_\theta z dz=\frac{h^3\Psi}{12(1-\nu^2)}(\kappa_\theta+\nu\kappa_r). \end{aligned}\right\} \tag{2.10}$$

Substituting Eqs. (2.6), (2.9) and (2.10) into the equation derived from Eq. (2.8) by operating $\Phi$, the following equation is obtained, where assumption (1) has been used.

$$\begin{aligned} h\Phi\Big[\bar{\sigma}_r R\beta+\bar{\sigma}_r\beta\frac{\partial^2 W}{\partial\beta^2}+\bar{\sigma}_\theta\Big(\frac{\partial W}{\partial\beta}+R\beta\Big)\Big] \\ -\frac{h^3\Psi}{12(1-\nu^2)R^2}\Big(\beta\frac{\partial^4 W}{\partial\beta^4}+2\frac{\partial^3 W}{\partial\beta^3}-\frac{1}{\beta}\frac{\partial^2 W}{\partial\beta^2}+\frac{1}{\beta^2}\frac{\partial W}{\partial\beta}\Big) \\ +R^2\beta\Phi\Big(q-hm\frac{\partial^2 W}{\partial t^2}\Big)=0. \end{aligned} \tag{2.11}$$

Eliminating $U$ from Eqs. (2.5), the compatibility equation is derived. Substituting Eqs. (2.3) into the equation obtained from the compatibility equation by operating $\Psi$, the following equation is obtained.

$$\Phi(1+\nu)(\bar{\sigma}_r-\bar{\sigma}_\theta)-\beta\Phi\Big(\frac{\partial\bar{\sigma}_\theta}{\partial\beta}-\nu\frac{\partial\bar{\sigma}_r}{\partial\beta}\Big)-\Psi\Big[\frac{\beta}{R}\frac{\partial W}{\partial\beta}+\frac{1}{2R^2}\Big(\frac{\partial W}{\partial\beta}\Big)^2\Big]=0. \tag{2.12}$$

Equation (2.7) is reduced to Eq. (2.13) in accordance with assumption (1).

$$\beta\frac{\partial\bar{\sigma}_r}{\partial\beta}+\bar{\sigma}_r-\bar{\sigma}_\theta=0. \tag{2.13}$$

Equation (2.13) can be satisfied by introducing stress function, $F$, defined by the relations,

This document is provided by JAXA.

$$\left.\begin{aligned}\left(\frac{R}{a}\right)\bar{\sigma}_r &= \frac{F}{\beta},\\ \left(\frac{R}{a}\right)\bar{\sigma}_\theta &= \frac{\partial F}{\partial \beta}.\end{aligned}\right\} \tag{2.14}$$

Using the stress function and nondimensional quantities defined by

$$\left.\begin{aligned}&\Phi_0 \equiv \Phi E, \quad \lambda \equiv 2[3(1-\nu^2)]^{1/4}(H/h)^{1/2},\\ &\tau \equiv (E/m)^{1/2}(t/R), \quad \xi \equiv (R/a)\beta, \quad p \equiv q/q_0,\\ &f \equiv F[12(1-\nu^2)a^2]/(Eh^2), \quad w \equiv 2[3(1-\nu^2)]^{1/2}(W/h),\end{aligned}\right\} \tag{2.15}$$

where $E$ is a constant which has a dimension of stress and

$$q_0 \equiv \{2E/[3(1-\nu^2)]^{1/2}\}(h/R)^2,$$

Equations (2.11) and (2.12) are reduced to

$$\Psi\xi\left[\frac{1}{\xi}\frac{\partial}{\partial\xi}\left(\xi\frac{\partial}{\partial\xi}\right)\right]^2 w - \Phi_0[\lambda^2(f\xi)' + (fw')' + \lambda^4(4p - \dot{w})\xi] = 0, \tag{2.16}$$

$$\Phi_0\xi\frac{\partial}{\partial\xi}\left[\frac{1}{\xi}\frac{\partial}{\partial\xi}(\xi f)\right] + \Psi[\tfrac{1}{2}(w')^2 + \lambda^2\xi w'] = 0, \tag{2.17}$$

where $(\ )'$ and $(\cdot)$ indicate the partial differentiation with respect to $\xi$ and $\tau$, respectively.

Equations (2.16) and (2.17) are the nonlinear governing equations for a viscoelastic shallow spherical shell for the case of axisymmetric deformation. They have been obtained from the conditions of equilibrium of forces; they can also be derived from a modified Hamilton's principle [*10*].

## 3. Response of Spherical Shells to Dynamic Loading

The behavior of viscoelastic shallow spherical shells with a clamped edge subjected to step and graded uniform pressures (Fig. 3) is analyzed.

### *3.1. Basic Equations and Boundary and Initial Conditions*

The basic equations are Eqs. (2.16) and (2.17), and the boundary conditions corresponding to a clamped edge condition are given by Eqs. (3.1) and (3.2).

at $\xi = 1$,
$$w = w' = 0, \tag{3.1}$$
$$U = 0. \tag{3.2}$$

Considering Eqs. (3.1) and (2.5), $\bar{\varepsilon}_\theta = 0$ $(\xi = 1)$ instead of Eq. (3.2) is used for analytical convenience' sake. Operating $\Psi$ on $\bar{\varepsilon}_\theta = 0$, the following equation is obtained.

$$\Phi_0(f' - \nu f) = 0. \tag{3.3}$$

This document is provided by JAXA.

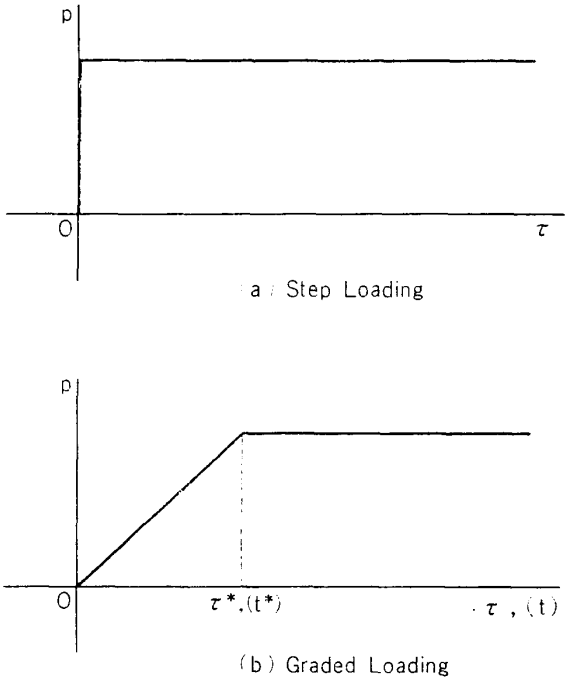


FIG. 3. Loading patterns.

Moreover, considering the conditions, i.e., $f=f'=0$ at $t=0$, Eq. (3.3) is equivalent to the following equation.

at $\xi=1$,

$$f'-\nu f=0. \tag{3.4}$$

Then the boundary conditions in the present analysis are given by Eqs. (3.1) and (3.4).

The deformation pattern, $w$, and the stress function, $f$, are an even and an odd function, respectively, and so they are expanded in terms of the Bessel function*.

$$w(\xi,\tau)=\sum_m a_m(\tau)w_m(\xi), \qquad m=1,2,3,\cdots, \tag{3.5}$$

$$f(\xi,\tau)=A_0(\tau)\xi+\sum_m b_m(\tau)J_1(\lambda_m\xi), \qquad m=1,2,3,\cdots, \tag{3.6}$$

where

$$w_m(\xi)=\frac{I_0(\alpha_m\xi)}{I_0(\alpha_m)}-\frac{J_0(\alpha_m\xi)}{J_0(\alpha_m)}. \tag{3.7}$$

* In the present analysis, the stress function, $f$, is expanded in terms of the Bessel function as shown in Eq. (3.6) in order to simplify the calculation. The value of stress function thus obtained is compared with one obtained by the finite difference method. The comparison is made also with the result by the Dini expansion, $f(\xi,\tau)=\sum_m g_m(\tau)J_1(\mu_m\xi)$, $m=1,2,3,\cdots$, where $\mu_m$'s are roots of $xJ_2(x)-(1-\nu)J_1(x)=0$ ($f'-\nu f=0$). The results by three methods differ little from one another, and it can be concluded that the present approximation is accurate enough. Full particulars will be reported separately.

This document is provided by JAXA.

To satisfy the boundary condition Eq. (3.1), the following relationship has to be held.

$$\frac{I_1(\alpha_m)}{I_0(\alpha_m)}+\frac{J_1(\alpha_m)}{J_0(\alpha_m)}=0. \tag{3.8}$$

And, the following equation is derived from Eqs. (3.4) and (3.6), where $\lambda_m$'s are roots of $J_1(x)=0$.

$$A_0(\tau)=\frac{-1}{1-\nu}\sum_m b_m(\tau)\lambda_m J_0(\lambda_m), \qquad m=1, 2, 3, \cdots. \tag{3.9}$$

Then, Eqs. (2.16) and (2.17) are solved approximately by the use of the Galerkin method under pertinent initial conditions.

Applying the Galerkin method to Eq. (2.16), and using the condition of orthonormality, that is, $\int_0^1 \xi w_m w_n d\xi=\delta_{mn}$ (1 for $m=n$, 0 for $m\neq n$) in the result, the following equations are given.

$$\begin{aligned}\lambda^4(\Phi_0\ddot{a}_n)+\alpha_n^4(\Psi a_n)&=\lambda^2\left\{\sum_m\left[\frac{2N_n}{\nu-1}V_m-C_{mn}\right](\Phi_0 b_m)\right\}\\&\quad-\sum_k\sum_m\left[\frac{1}{\nu-1}V_k D_{mn}+E_{mkn}\right]\Phi_0(b_k a_m)+4\lambda^4 N_n(\Phi_0 p),\end{aligned} \tag{3.10}$$

where

$$\left.\begin{aligned}&V_m=\lambda_m J_0(\lambda_m), \quad N_n=\int_0^1 \xi w_n d\xi,\\&C_{mn}=\alpha_n^4\lambda_m J_0(\lambda_m)N_n/(\lambda_m^4-\alpha_n^4), \quad E_{mkn}=\int_0^1 J_1(\lambda_k\xi)w_m' w_n' d\xi,\\&D_{mn}=-(\alpha_m\alpha_n)^2[(N_m-N_n)/(\alpha_m^2-\alpha_n^2)-(N_m+N_n)/(\alpha_m^2+\alpha_n^2)], \quad (m\neq n),\\&\quad=(\alpha_m^2 N_m)^2/4, \quad (m=n).\end{aligned}\right\} \tag{3.11}$$

Applying the Galerkin method to Eq. (2.17), the following equations are obtained.

$$\Phi_0 b_n(\tau)=\frac{\Psi}{V_n^2}\left(2\lambda^2\sum_m a_m C_{nm}+\sum_s\sum_t E_{snt}a_s a_t\right). \tag{3.12}$$

In the present analysis, Eqs. (3.10) and (3.12), derived from Eqs. (2.16) and (2.17), instead of Eqs. (2.3) through (2.10) inclusive, are to be solved, and so the additional (initial) conditions have to be taken into consideration. For the present case, the conditions,

at $t=0$, $$q-hm\frac{\partial^2 W}{\partial t^2}=0, \quad \text{and} \quad F=0, \tag{3.13}$$

$$\frac{\partial^2 W}{\partial t^2}=0, \quad \text{and} \quad F=0, \tag{3.14}$$

This document is provided by JAXA.

have to be added for the cases of step and graded loadings, respectively, to the initial conditions,

$$\text{at } t=0, \qquad w=\dot{w}=0. \tag{3.15}$$

In the former loading case, it is so difficult to satisfy exactly the additional initial condition $q-hm\partial^2 W/\partial t^2=0$ that the condition is satisfied approximately by the use of the Galerkin procedure.

In carrying out the numerical analysis, the three-element model in Fig. 2(a) is used to describe the viscoelastic characteristics of the material, then $\Phi$ and $\Psi$ in Eqs. (2.2) are expressed as follows.

$$\left.\begin{aligned} &\Phi\equiv\frac{1}{E_0}+\left(\frac{\tau_2}{E_1}\right)\frac{\partial}{\partial t}, \quad \Psi\equiv 1+\tau_2\frac{\partial}{\partial t}, \\ &\frac{1}{E_0}\equiv\frac{1}{E_1}+\frac{1}{E_2}, \quad \tau_2\equiv\frac{\eta_2}{E_2}. \end{aligned}\right\} \tag{3.16}$$

Systems which are expressed by a four-element model and so on can be analyzed in the similar way.

In the following, using the Runge-Kutta-Gill procedure, the behavior of the system subject to the basic equations (3.10) and (3.12) and the initial conditions mentioned above are obtained numerically by approximating both $w$ and $f$ with four or eight terms (the time step: $\Delta\tau=0.01$).

### 3.2. *Dynamic Behavior of Shells*

In obtaining numerical solutions, the following quantities are used, that is,

$$\begin{aligned} &E_1=418\ \text{kg/mm}^2, \quad E_2=1640\ \text{kg/mm}^2, \quad E=418\ \text{kg/mm}^2, \\ &\lambda=5, \quad \nu=1/3, \quad mg=1.19\ \text{gr/cm}^3, \quad R=1000\ \text{mm}, \\ &a=150\ \text{mm}, \end{aligned}$$

where the value $\nu=1/3$ has been used to compare the results with previous works.

Some of the results of numerical solutions are shown in Figs. 4 and 5.

Figure 4 shows the variation of mean deformation, $\rho$, with time, $\tau$, with the retardation time, $\tau_2$, as a parameter, for the case of step loading. It is seen in Fig. 4 that the smaller $\tau_2$ becomes, the more quickly the large deformation response appears and that values of $\rho$ before buckling increase monotonically with the decrease in $\tau_2$. However, the first peak value of $\rho$ at buckling, $\rho_{\max}$, does not change monotonically with $\tau_2$, that is, in the present numerical example, it has the local minimum value in the vicinity of $\tau_2=7$ msec. In another example ($p=0.7$) shown in Table 1, $\rho_{\max}$ increases monotonically with the decrease in $\tau_2$. This phenomena are subjected to effects of both creeping and damping characteristics in the three-element viscoelastic model.

In Fig. 5, the change of dynamic buckling loads, $p_c$, with the loading speed, $dp/d\tau$, is shown. It is seen in Fig. 5 that when $(dp/d\tau)^{-1}$ is larger than about 10, that is, $t^*$ (Fig. 3) is larger than about 2.5 msec in the present numerical example,

This document is provided by JAXA.

the phenomena are no longer of dynamic but are nearly equal to that of quasi-static. The present criterion of buckling is based on whether a shell snaps through or not, but when the loading speed is slow, $p_c$ for some ranges of $\tau_2$ becomes higher than the static buckling load ($E_0$), $p_{s0}$, (Fig. 5), so a new criterion in such cases has to be introduced which will be discussed later.

The effect of $\tau_2$ on $p_c$ has the tendency similar to that of $(dp/d\tau)^{-1}$, and $p_c$ changes markedly for values of $\tau_2$ near zero. However, as far as the dynamic response is

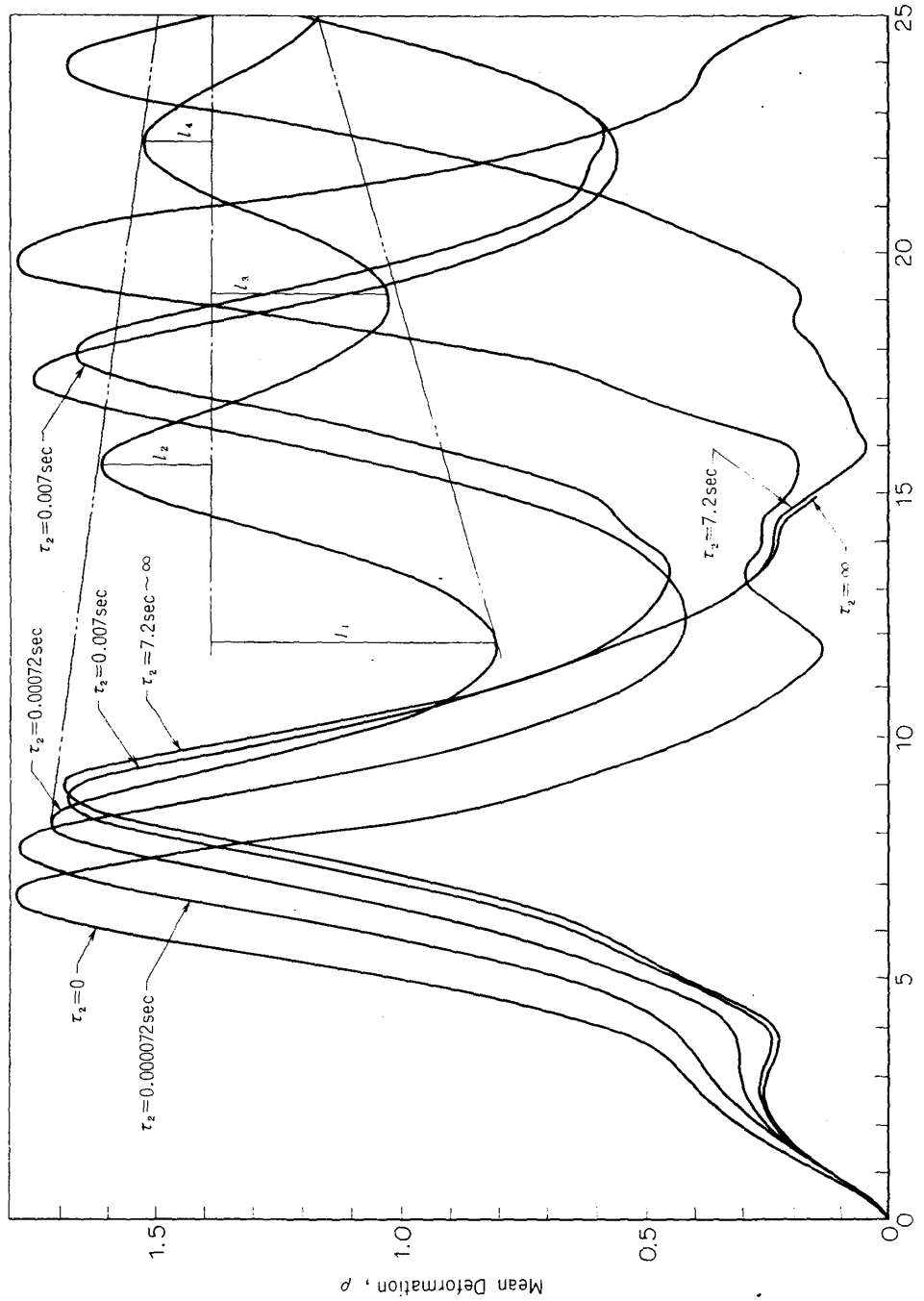


FIG. 4. Change of mean deformation with time; step loading, $p$=0.60, $\lambda$=5.0.

This document is provided by JAXA.

TABLE 1. Change of $\rho_{max}$ with retardation time, $\tau_2$; $(dp/d\tau)^{-1}=1.0$, $\lambda=5.0$.

| $p$ | $\tau_2$ (sec) | $\rho_{max}$ | $\tau(\rho=\rho_{max})$ |
|---|---|---|---|
| 0.70 | 7.2 | 1.767 | 7.5 |
| | 0.007 | 1.768 | 7.5 |
| | 0.00072 | 1.781 | 7.2 |
| 0.65 | 7.2 | 1.726 | 8.3 |
| | 0.007 | 1.720 | 8.2 |
| | 0.00072 | 1.759 | 7.8 |

concerned, $\tau_2$ does not always have an effect similar to that of $(dp/d\tau)^{-1}$, because in the dynamic response the viscous damping plays an increasingly apparent role, that is, the postbuckling damping behavior changes monotonically with $(dp/d\tau)^{-1}$ and not with $\tau_2$ (Fig. 4).

From Fig. 5, for the cases with values of $\tau_2$ larger than several msec (the value of $\tau_2$ of actual hypolymer is of this range), it seems reasonable that the problem may be dealt with as that of elastic shells whose Young's modulus is the instantaneous modulus, $E_1$, as long as only the dynamic buckling load is concerned.

$l_n$'s $(n=1, 2, 3, \cdots)$ in Fig. 4 are the differences between the value of $\rho(\infty)$ and the every peak value of $\rho(\tau)$. The values of decrement ratio $(l_{n+2}/l_n)$ are nearly constant and so the variation of $(l_3/l_1)$ with $\tau_2$ is plotted in Fig. 6. Figure 6 can be used to estimate the effect of retardation time on the damping characteristics of the motion after buckling.

In Figs. 4 and 6, for the case of $\tau_2=\infty$, the response of shells is that of elastic shells with $E_1$, and the smaller $\tau_2$ becomes (up to about 720$\mu$sec in the present numerical example), the larger the effect of damping is, and thereafter the effect of damping decreases and finally the response of shells results in that of elastic shells with Young's modulus $E_0$.

In order to observe the response of viscoelastic spherical shells to dynamic loading and to check the results of the numerical solution, some experiments have been carried out.

In Fig. 7, an example of the changes of circumferential strains with time is shown. The strains have been measured by resistant-wire strain gauges adhesive-bonded on the shell surface at three symmetrical points on a circle. It is seen from Fig. 7 that the deformation of the shell is axisymmetrical, and it confirms assumption (4) given in Section 2 for shells within the range of geometrical parameter considered in the present analysis. One of the experimental results is compared with the theoretical result in Fig. 8. As shown in this figure, a good agreement between the theoretical and experimental values has been observed up to point A which corresponds to the first maximum value of $\rho$.

From the numerical and experimental results, the following explanations in ad-

This document is provided by JAXA.

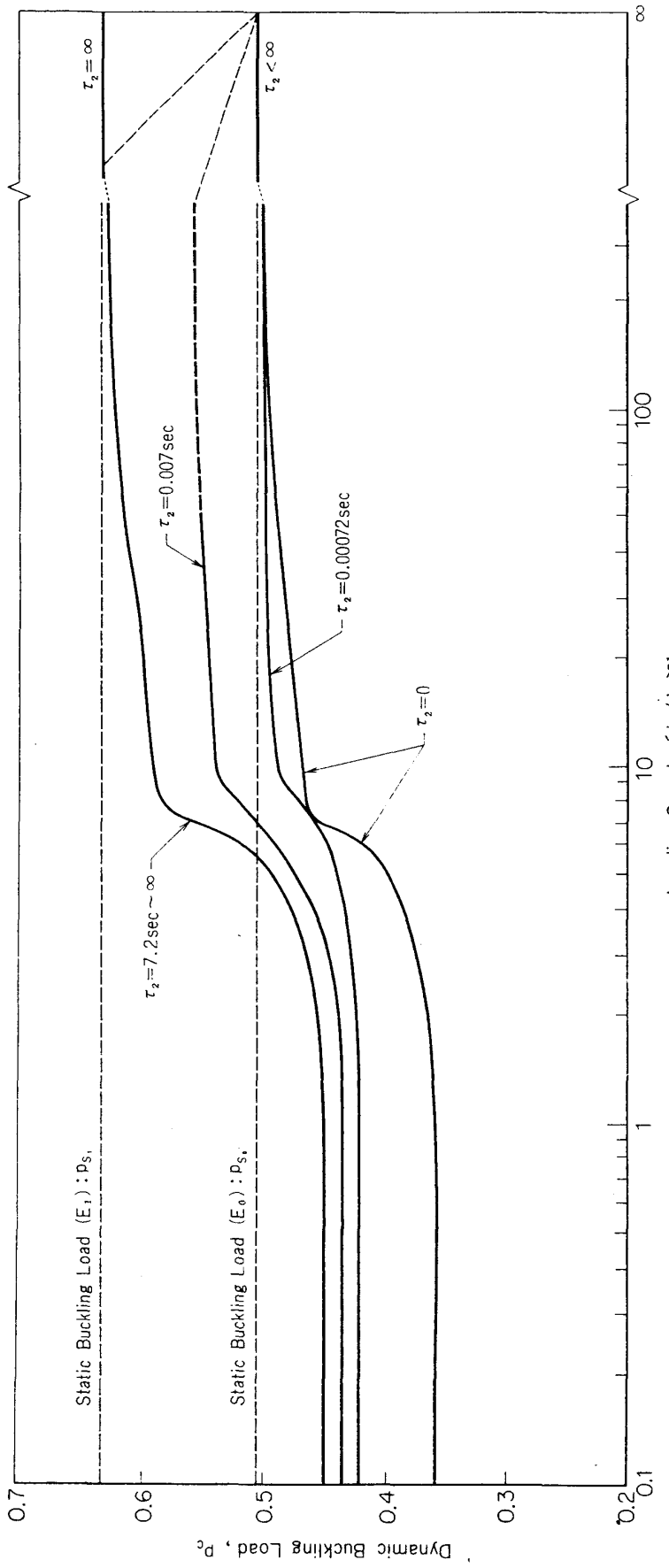


FIG. 5. Dynamic buckling load; $\lambda=5.0$.

This document is provided by JAXA.

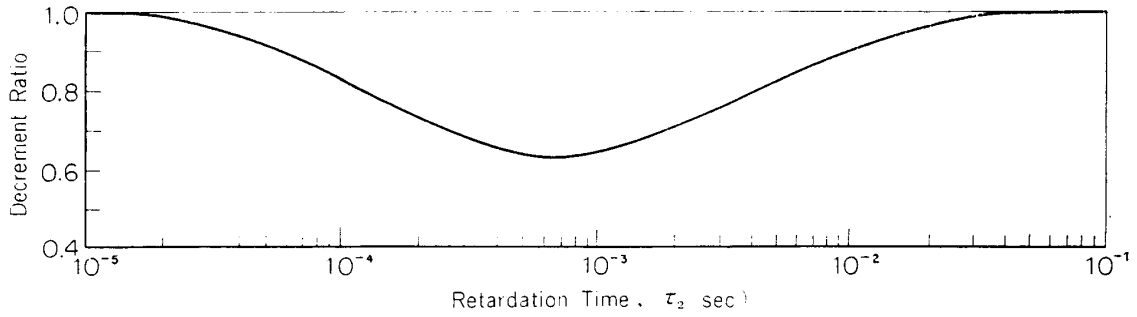


FIG. 6. Change of decrement ratio after dynamic buckling with retardation time; step loading, $p=0.60$, $\lambda=5.0$.

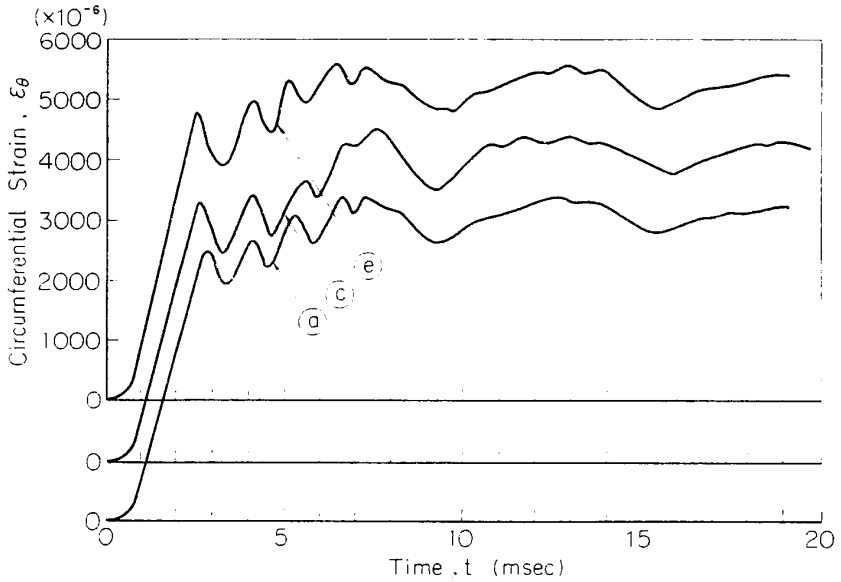


FIG. 7. Change of circumferential strains with time; an experimental result, buckled case, $p=0.433$, $(dp/d\tau)^{-1}\simeq 4$, $\lambda=4.75$, $\tau_2=14.0$ sec.

dition to those stated above are given for the problem.

1) critical load:

In the present paper, both step and graded loadings are taken into account, and the snap-through load has been presumed as the critical load.

In determining the critical load, it is necessary to introduce some considerations for cases where a) the dynamic buckling load, $p_c$, seems to be higher than the static buckling load $(E_0)$, $p_{s0}$, and b) the effect of damping seems to be small.

In the former case, $p_c$ is determined in the way as shown in Fig. 9. That is, the values of the ordinate corresponding to cusps in Fig. 9 have been considered as $p_c$. The fact that there exist cusps on curves in Fig. 9 means that there are two regions where the effect of creep appears predominantly and where it does not, and it has been confirmed by both numerical estimations and experimental evidences that in the left-hand region of the cusp the dynamic buckling occurs and in the right-hand region the creep buckling. This is the reason why $p_c$ has been

This document is provided by JAXA.

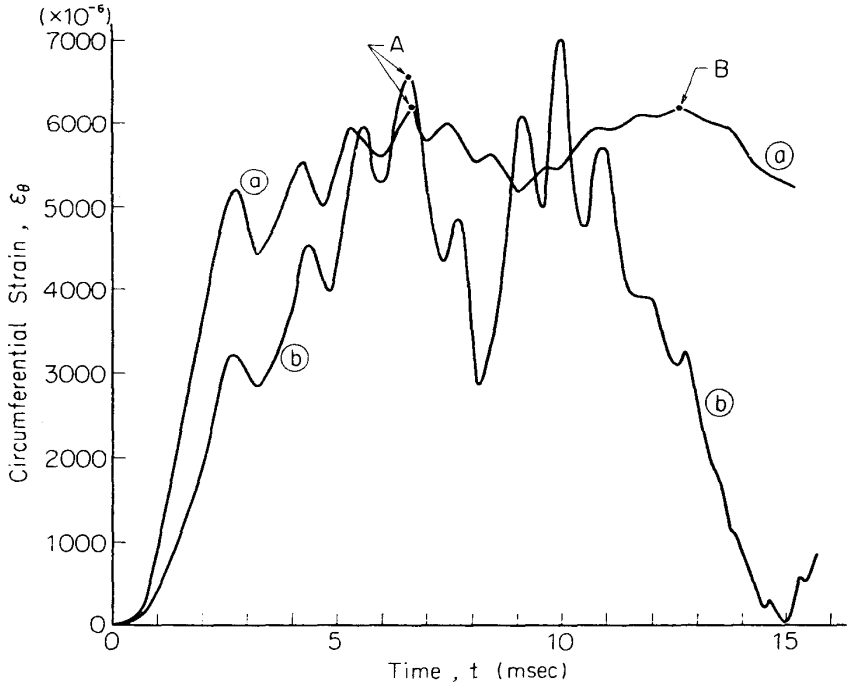


FIG. 8. Change of circumferential strains with time; $p/p_c=1.023$, $\lambda=4.75$, $\tau_2=14.0$ sec, $E_1=400$ kg/mm², $E_2=1470$ kg/mm².
ⓐ: an experimental result, $(dp/d\tau)^{-1}\simeq 4$, ⓑ: a numerical result, $(dp/d\tau)^{-1}=4$.

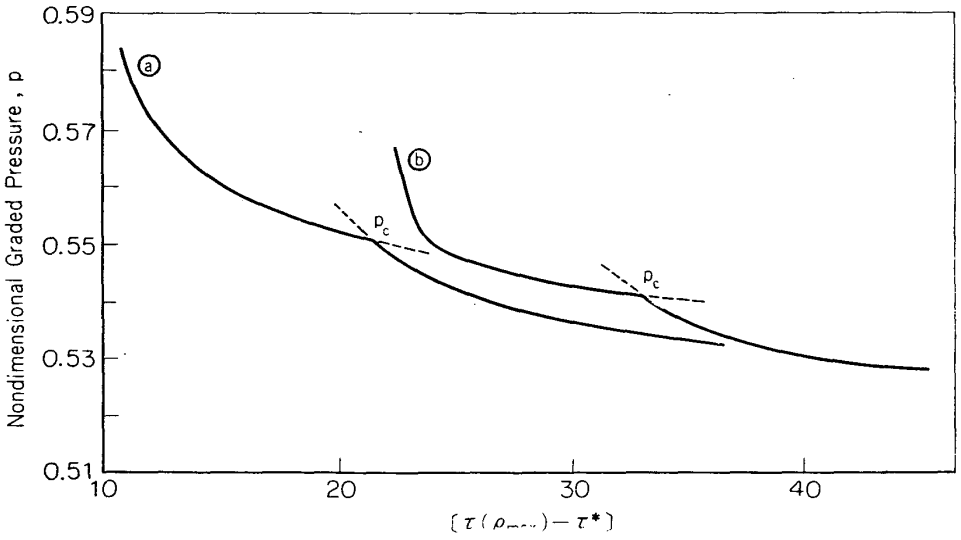


FIG. 9. Change of the time, $[\tau(\rho_{max})-\tau^*]$ with load; $\lambda=5.0$, $\tau_2=7$ msec.
ⓐ: $(dp/d\tau)^{-1}=10$, ⓑ: $(dp/d\tau)^{-1}=50$.

determined in the way mentioned above. An example of the experimental results for the case where the buckling accompanied with creep deformation occurs is shown in Fig. 10.

In the latter case, there are a few regions of load where the shell does not buckle

This document is provided by JAXA.

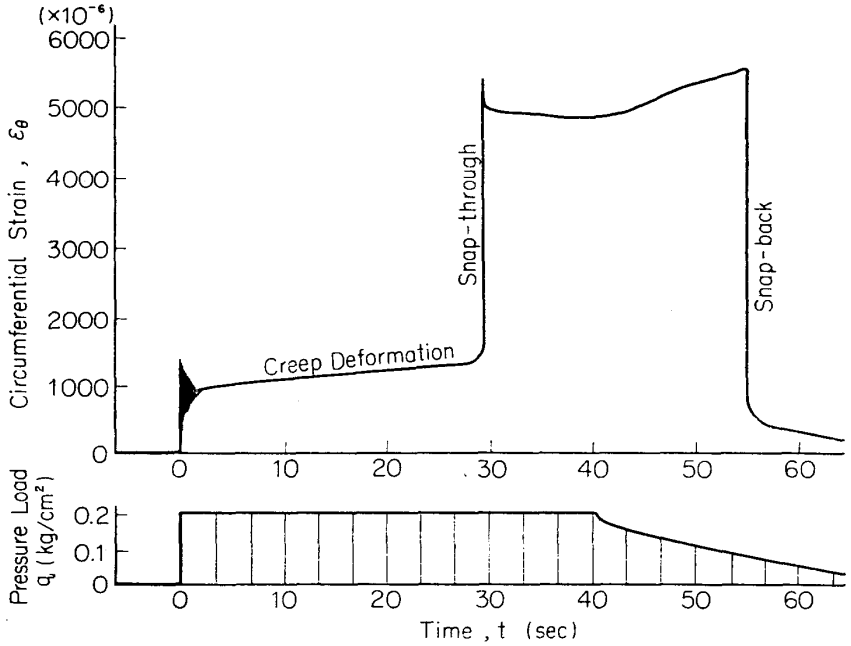


FIG. 10. Change of circumferential strain with time, an experimental result, buckled case accompanied with creep deformation; $q=0.217$ kg/cm², $(dp/d\tau)^{-1}\simeq 4$, $\lambda=4.88$, $\tau_2=14.0$ sec.

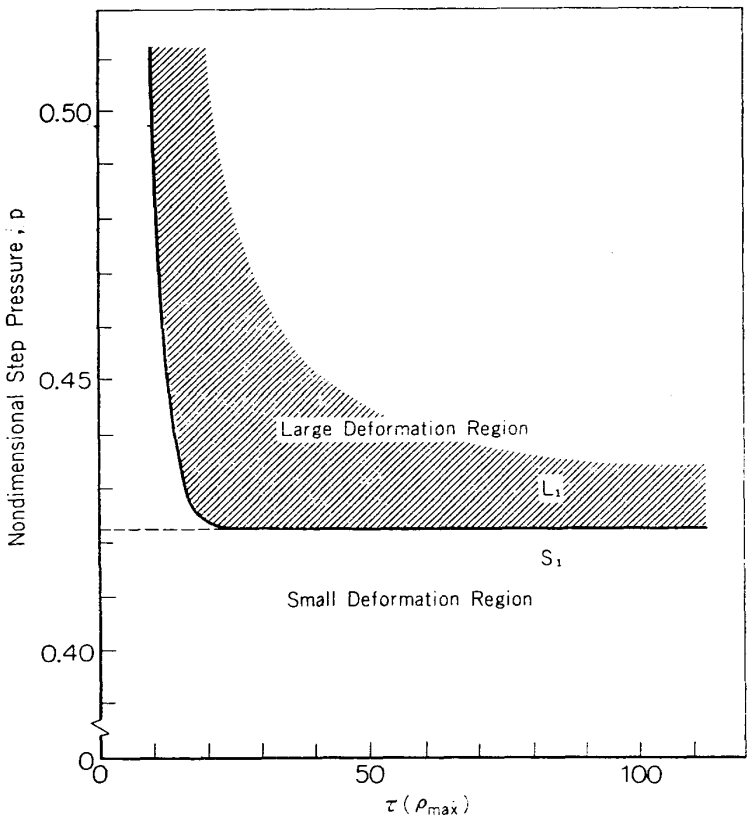


FIG. 11. Degree of ease in generating large deformation; step loading, $\lambda=5.0$, $\tau_2=720$ μsec.

This document is provided by JAXA.

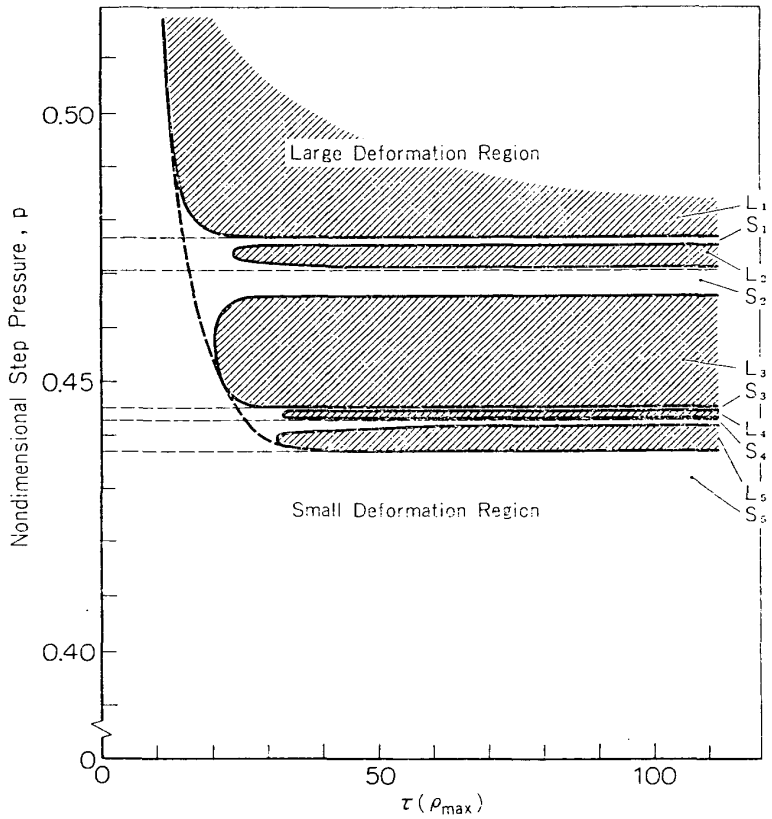


FIG. 12. Degree of ease in generating large deformation; step loading, $\lambda=5.0$, $\tau_2=7$ msec.

dynamically in a limited time as shown in Figs. 11, 12 and 22. A similar result has also been derived by the authors from Huang's procedure (1969), although he has not mentioned about it. And, the lowest load of loads which are sufficient to generate snap-through in the shell is adopted as $p_c$.

It can be seen from both cases that it is important to consider the role of time in analyzing the problems similar to those treated in the present paper.

The critical loads shown in Fig. 5 are based on this concept, including the considerations mentioned above.

2) motion of viscoelastic shells:

In Figs. 11 and 12, $L_n$'s ($n=1, 2, \cdots, 5$) indicate large deformation regions, while $S_n$'s small deformation regions. And, Fig. 13 shows the variation of the response of viscoelastic shells with the loaded step pressure and retardation time.

The motion of viscoelastic shells subjected to step loading in some of the above-mentioned regions are shown in Figs. 14 to 18 inclusive, where figures in circles correspond to those in Fig. 13. Figures 14 and 15 show motions of viscoelastic shell in the same large deformation region, $L_1$. Figures 16 and 17 show motions of viscoelastic shell in the large deformation regions, $L_1$ and $L_3$, respectively. The difference in loaded pressures between the cases in Figs. 14 and 15 is nearly equal to that between the cases in Figs. 16 and 17. Although motions in Figs. 14 and 15 are similar to each other, those in Figs. 16 and 17 are not. From this evidence,

This document is provided by JAXA.

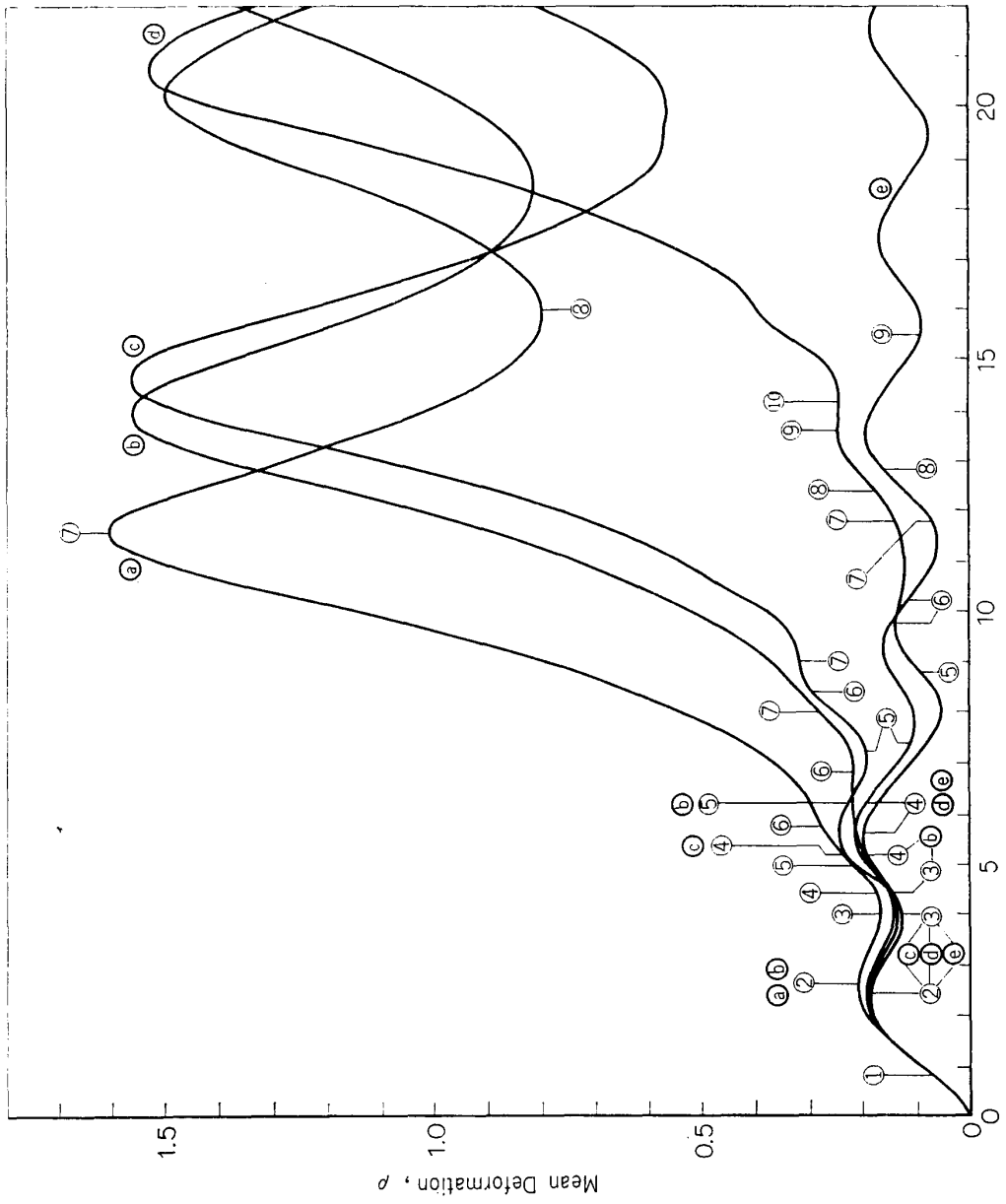


FIG. 13. Response of viscoelastic shells; step loading, $\lambda=5.0$.
ⓐ : $p=0.470$, $\tau_2=720$ $\mu$sec, ⓑ : $p=0.440$, $\tau_2=720$ $\mu$sec, ⓒ : $p=0.485$, $\tau_2=7$ msec,
ⓓ : $p=0.460$, $\tau_2=7$ msec, ⓔ : $p=0.470$, $\tau_2=7$ msec.

This document is provided by JAXA.

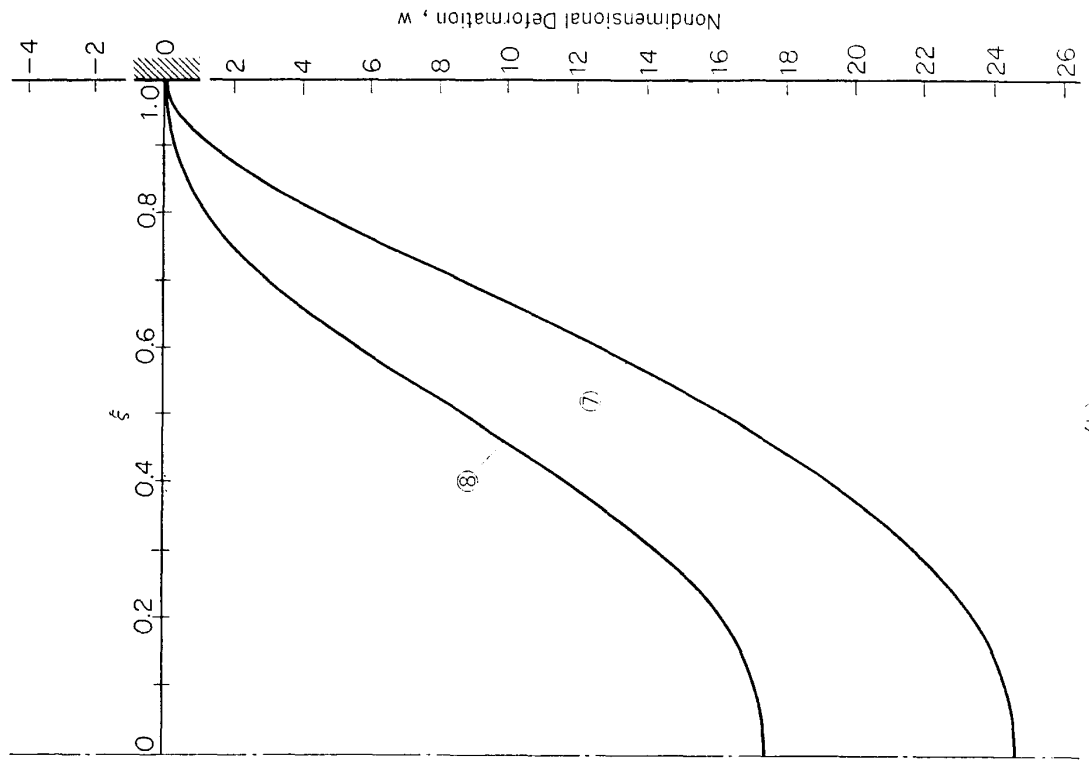


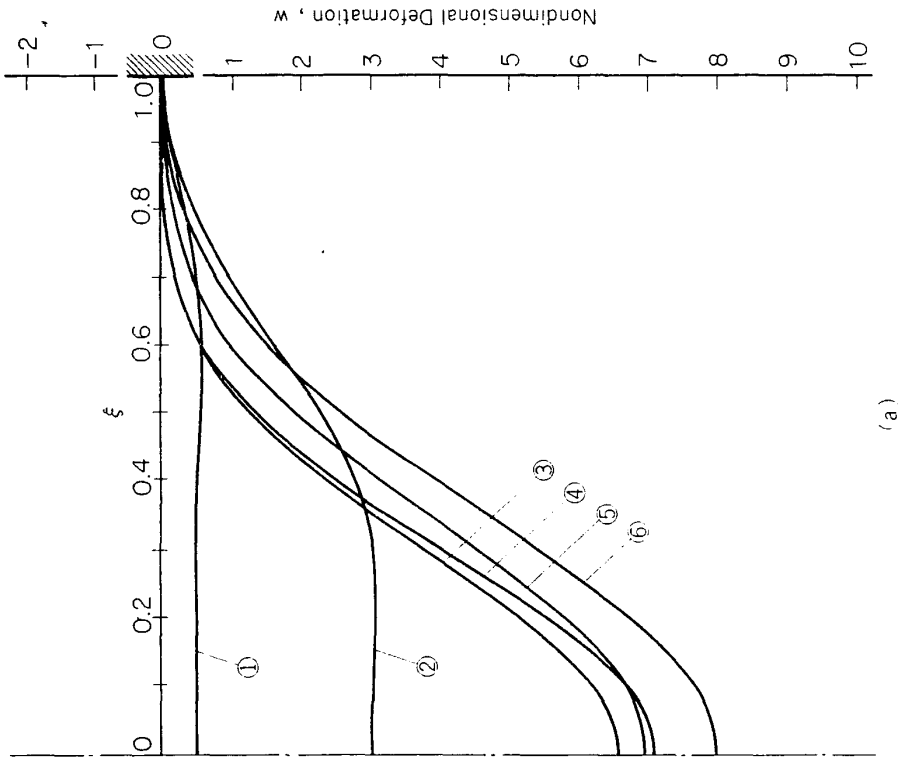


FIG. 14. Motion of a viscoelastic shell; step loading, $p=0.470$, $\lambda=5.0$, $\tau_2=720\ \mu sec$.
(a) before buckling
(b) after buckling

This document is provided by JAXA.

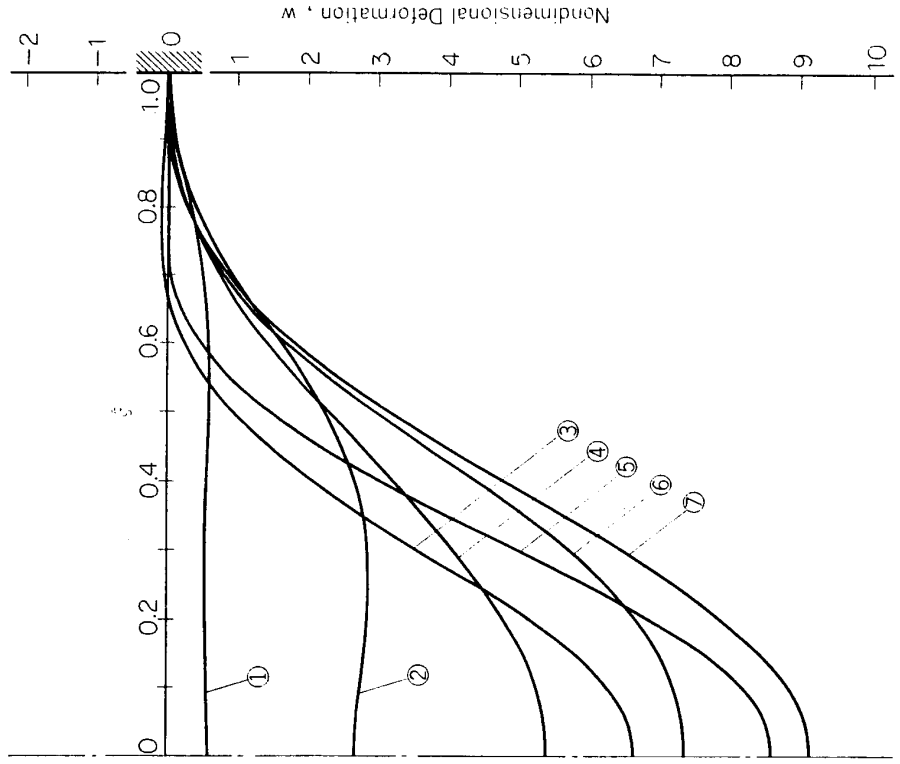


FIG. 16. Motion of a viscoelastic shell; step loading, $p=0.485$, $\lambda=5.0$, $\tau_2=7$ msec.

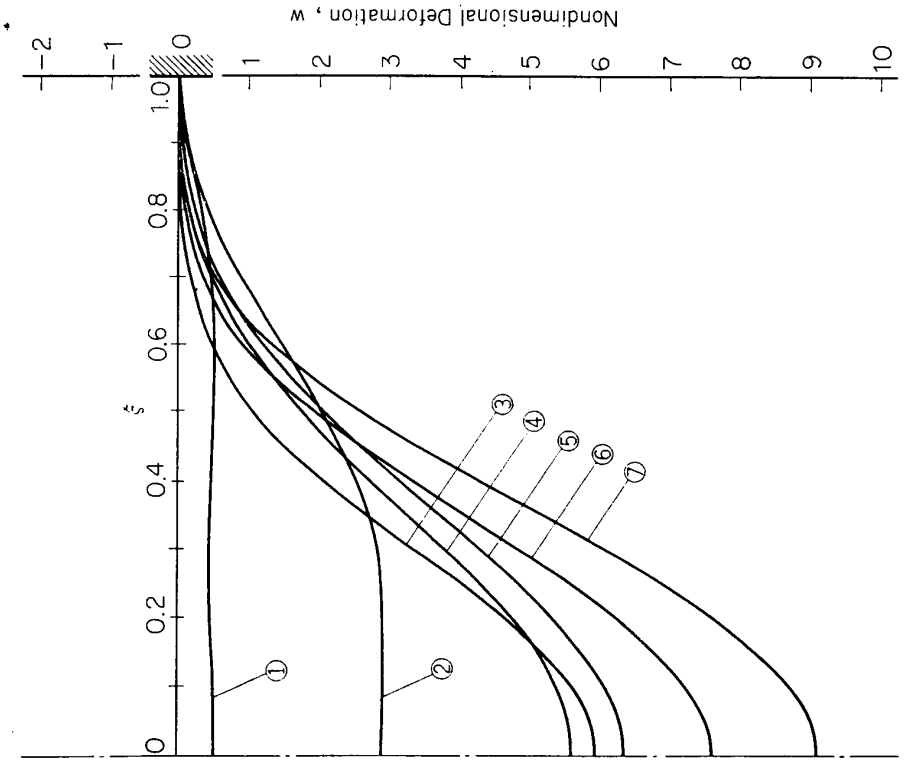


FIG. 15. Motion of a viscoelastic shell; step loading, $p=0.440$, $\lambda=5.0$, $\tau_2=720$ $\mu$sec.

This document is provided by JAXA.

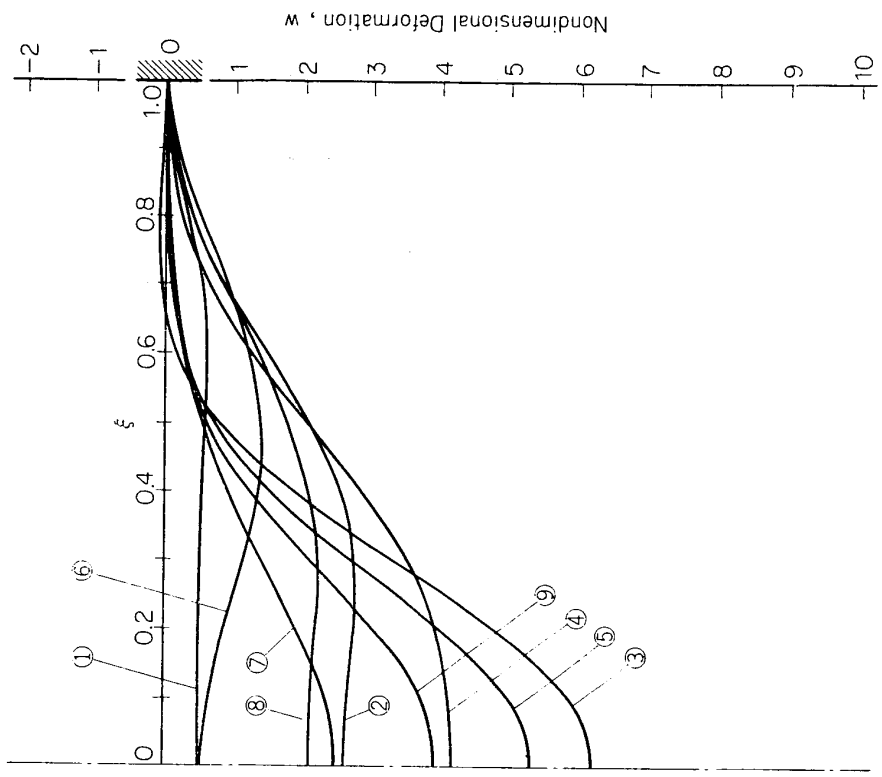


FIG. 18. Motion of a viscoelastic shell; step loading, $p=0.470$, $\lambda=5.0$, $\tau_2=7$ msec.

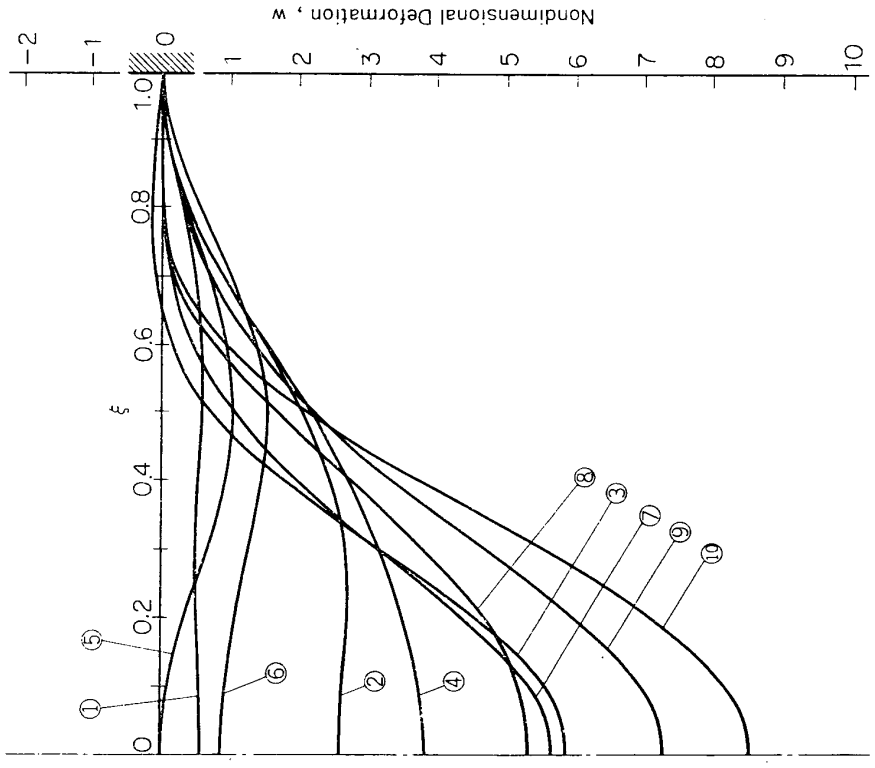


FIG. 17. Motion of a viscoelastic shell; step loading, $p=0.460$, $\lambda=5.0$, $\tau_2=7$ msec.

This document is provided by JAXA.

it can be concluded that the motion of viscoelastic shells in the same region is substantially the same.

Moreover, it can be seen in Fig. 14(b) that the buckled pattern is almost formed up by the first mode only.

The every local extremal value of $\rho(\tau)$ in Fig. 13 corresponds in general to that of $w(0, \tau)$ in Figs. 14 to 18 inclusive, respectively. This fact shows that it is pertinent to analyze the motion of shells using the relationship $\rho(\tau)$ vs. $\tau$ instead of $w(0, \tau)$ vs. $\tau$.

3) effect of viscoelasticity:

The effect of viscoelasticity on the critical load can be seen in Figs. 4 and 5. Results shown in Figs. 4 and 5 have the tendency similar to that shown by Huang and Nachbar (1968) for the case of viscoelastic shallow arches.

The phenomena that modes of higher order are suppressed by the viscoelastic effect can be easily examined by the comparison of amplitudes.

From the numerical solutions presented, it can be seen that the loading speed and retardation time have significant effects on the dynamic buckling load over a limited range of their values.

4) quasi-static buckling load:

It is shown in Figs. 4 and 6 that the maximum damping appears for the case of $\tau_2=720$ $\mu$sec in the present numerical solution. Multiplying $p_{s0}=0.500$ [at $(dp/d\tau)^{-1}=200$] for the above case by $E_1/E_0$, obtained is the quasi-static buckling load $p_{s1}=p_{s0}(E_1/E_0)=0.628$, which differs little from the static buckling load, e.g., by only 0.16% from that obtained by Thurston (1961).

## 4. Concluding Remarks

In the present paper, the axisymmetric dynamic behavior of viscoelastic shallow spherical shells with a clamped edge has been analyzed.

The nonlinear governing equations of the problem have been derived first of all, representing the viscoelastic characteristics of materials by a linear model. Then the equations have been solved numerically for the cases of step and graded loadings.

The relationships between the dynamic loads and the resulting responses have been obtained for the shell of specified geometrical parameter, and the critical load and the effects of viscoelasticity and loading speed on the dynamic behavior of shells have been discussed, paying special attention to the role of time. And a clear definition of dynamic buckling has been proposed.

Some experimental results have been presented and a good agreement between the theoretical predictions and experimental results has been shown.

It is natural that the quasi-static buckling load obtained from the present results has coincided with the corresponding static one.

The present procedure can be applied easily to problems of elastic shells and some solutions will be shown in the APPENDIX.

The numerical computations were carried out on the HITAC 5020F computer

This document is provided by JAXA.

of The University of Tokyo, operating double precision.

The present paper is the English version of extracts from References [*11*] and [*12*].

*Department of Structures,*
*Institute of Space and Aeronautical Science,*
*The University of Tokyo.*
*November 20, 1974.*

## REFERENCES

[*1*] Archer, R. R. & Lange, C. G.: Nonlinear Dynamic Behavior of Shallow Spherical Shells, AIAA J., **3** (1965), 2313–2317.
[*2*] Budiansky, B. & Roth, R. S.: Axisymmetric Dynamic Buckling of Clamped Shallow Spherical Shells, NASA, TN D-1510, (1962), 597–606.
[*3*] Chao, C. & Achenbach, J. D.: A Simple Viscoelastic Analogy for Stress Waves, "Stress Waves in Anelastic Solids", ed. H. Kolsky and W. Prager, Springer-Verlag, Berlin, (1964), 222–238.
[*4*] Chiu, S.-S. & Neubert, V. H.: Difference Method for Wave Analysis of the Split Hopkinson Pressure Bar with a Viscoelastic Specimen, Jour. Mech. Phys. Solids, **15** (1967), 177–193.
[*5*] Evensen, H. A. & Evan-Iwanowski, R. M.: Dynamic Response and Stability of Shallow Spherical Shells, Subjected to Time-Dependent Loading, AIAA J., **5** (1967), 969–976.
[*6*] Huang, N.-C. & Nachbar, W.: Dynamic Snap-Through of Imperfect Viscoelastic Shallow Arches, Jour. Appl. Mech., **35** (1968), 289–296.
[*7*] Huang, N.-C.: Axisymmetric Dynamic Snap-Through of Elastic Clamped Shallow Spherical Shells, AIAA J., **7** (1969), 215–220.
[*8*] Humphreys, J. S. & Bodner, S. R.: Dynamic Buckling of Shallow Shells under Impulsive Loads, Jour. Engng. Mech. Div., Proc. ASCE, 88 (1962), EM 2, 17–36.
[*9*] Kobayashi, A.: An Investigation of Creep Bending Characteristics of Linear Polymer Column Influenced by Non-Uniform Thermal Environments, Inst. Space Aeron. Sci., The University of Tokyo, Report, **31** (1966), 31–43.
[*10*] Kumai, N.: Dynamic Response of a Viscoelastic Shallow Spherical Shell, Master's Thesis, The University of Tokyo, (1970).
[*11*] Kumai, N. & Sunakawa, M.: Response of Viscoelastic Shallow Spherical Shells to Dynamic Pressures, Jour. Japan Soc. Aeron. Space Sci., **19** (1971), 452–465. (in Japanese)
[*12*] Kumai, N. & Sunakawa, M.: Dynamic Response of Viscoelastic Shallow Spherical Shells, Inst. Space Aeron. Sci., The University of Tokyo, Bulletin, 8-2(B) (1972), 355–376. (in Japanese)
[*13*] Liepins, A. A.: Asymmetric Nonlinear Dynamic Response and Buckling of Shallow Spherical Shells, NASA, CR-1376, (1969).
[*14*] Lock, M. H., Okubo, S. & Whitter, J. S.: Experiments on the Snapping of a Shallow Dome Under a Step Pressure Load, AIAA J., **6** (1968), 1320–1326.
[*15*] Simitses, G. J.: Axisymmetric Dynamic Snap-Through Buckling of Shallow Spherical Caps, ibid., **5** (1967), 1019–1021.
[*16*] Sunakawa, M. & Kumai, N.: Response of Structural Components to Dynamic Loading, Jour. Japan Soc. Aeron. Space Sci., **18** (1970), 154–166. (in Japanese)
[*17*] Sunakawa, M.: A Note on the Stability of Shells, "Theoretical and Applied Mechanics", **22** (1974), 17–32.
[*18*] Suzuki, S.: The Effect of Solid Viscosities to Dynamic Load Factors of the Ring and the Hollow Sphere Subjected to Impulsive Loads, Aeron. Jour., **72** (1968), 971–976.
[*19*] Thurston, G. A.: A Numerical Solution of the Nonlinear Equations for Axisymmetric Bending of Shallow Spherical Shells, Jour. Appl. Mech., **28** (1961), 557–562.

This document is provided by JAXA.

## APPENDIX

## DYNAMIC BEHAVIOR OF ELASTIC SHELLS

The dynamic behavior of an elastic shallow spherical shell obtained by the present procedure is compared in Fig. 19 with some of previous results, and an excellent agreement among them is seen except the one by Budiansky and Roth (1962), which seems to have some error in the numerical calculation.

The results by the present procedure by the four-term and eight-term approximations and the solution by the finite difference method for the response of an elastic shell are shown in Fig. 20. From this figure, it can be seen that the four-term approximation is highly precise. The motion of an elastic shell subjected to step loading is shown in Figs. 21, where figures in circles correspond to those in Fig. 20. Comparing motions in Figs. 21 and 17, the effect of damping can be observed apparently (especially, ⑦ in the former and ⑤ in the latter).

Degree of ease in generating large deformation is shown in Fig. 22. There are two large deformation regions in this elastic case contrary to Fig. 11, where the

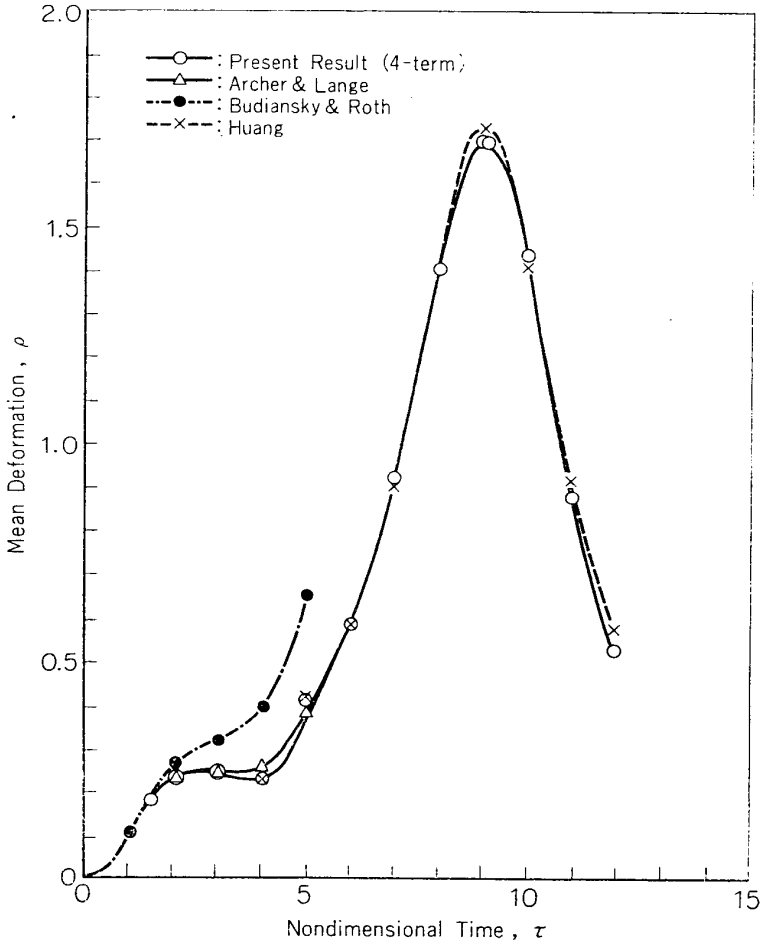


FIG. 19. Comparison of $\rho(\tau)$ vs. $\tau$ curves; step loading, $p=0.60$, $\lambda=5.0$, $\tau_2=\infty$.

This document is provided by JAXA.

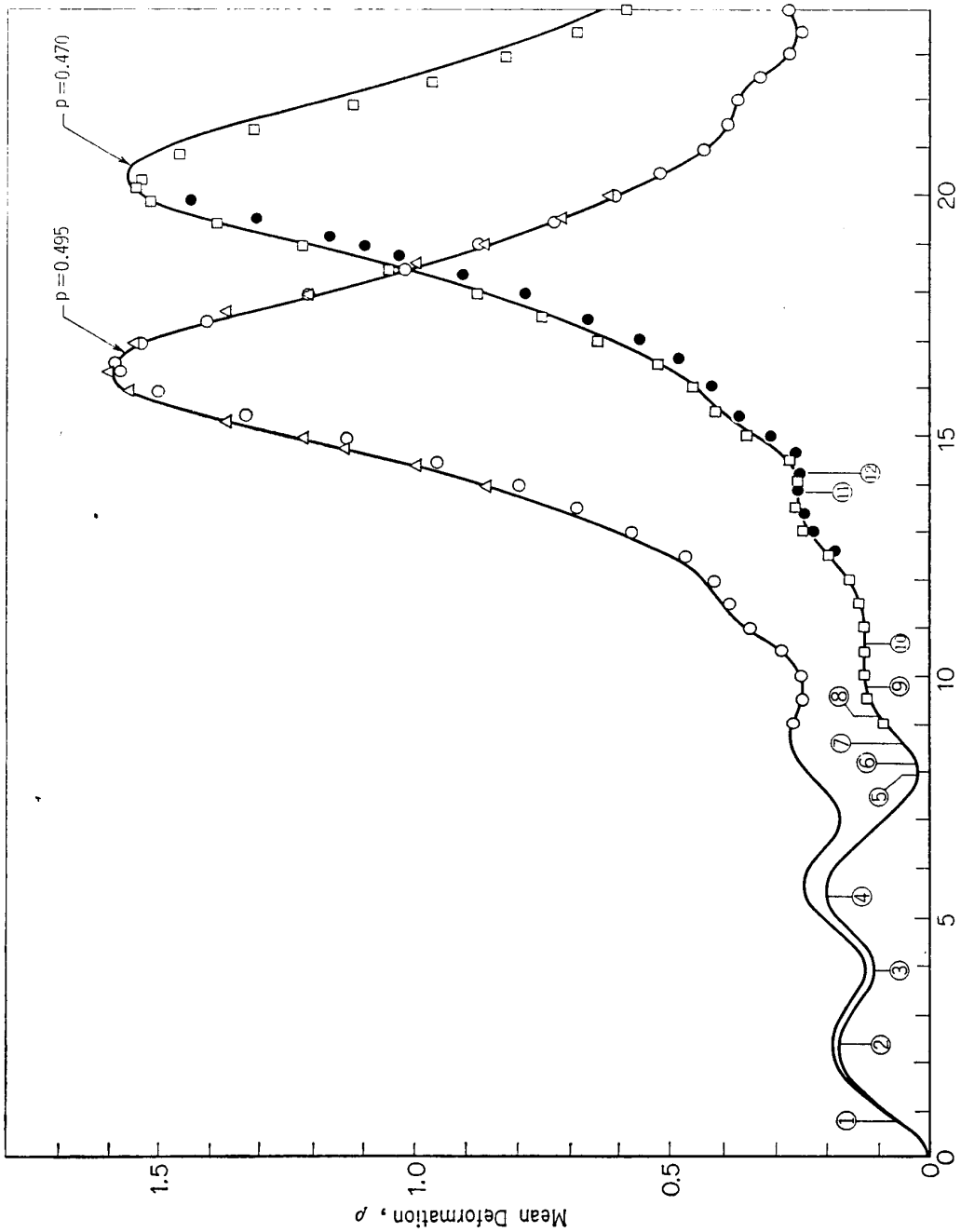


FIG. 20. Response of an elastic shell; step loading, $\lambda=5.0$, $\tau_2=\infty$.
—: eight-term approx. ○, □: four-term approx. △, ●: finite difference method.

This document is provided by JAXA.

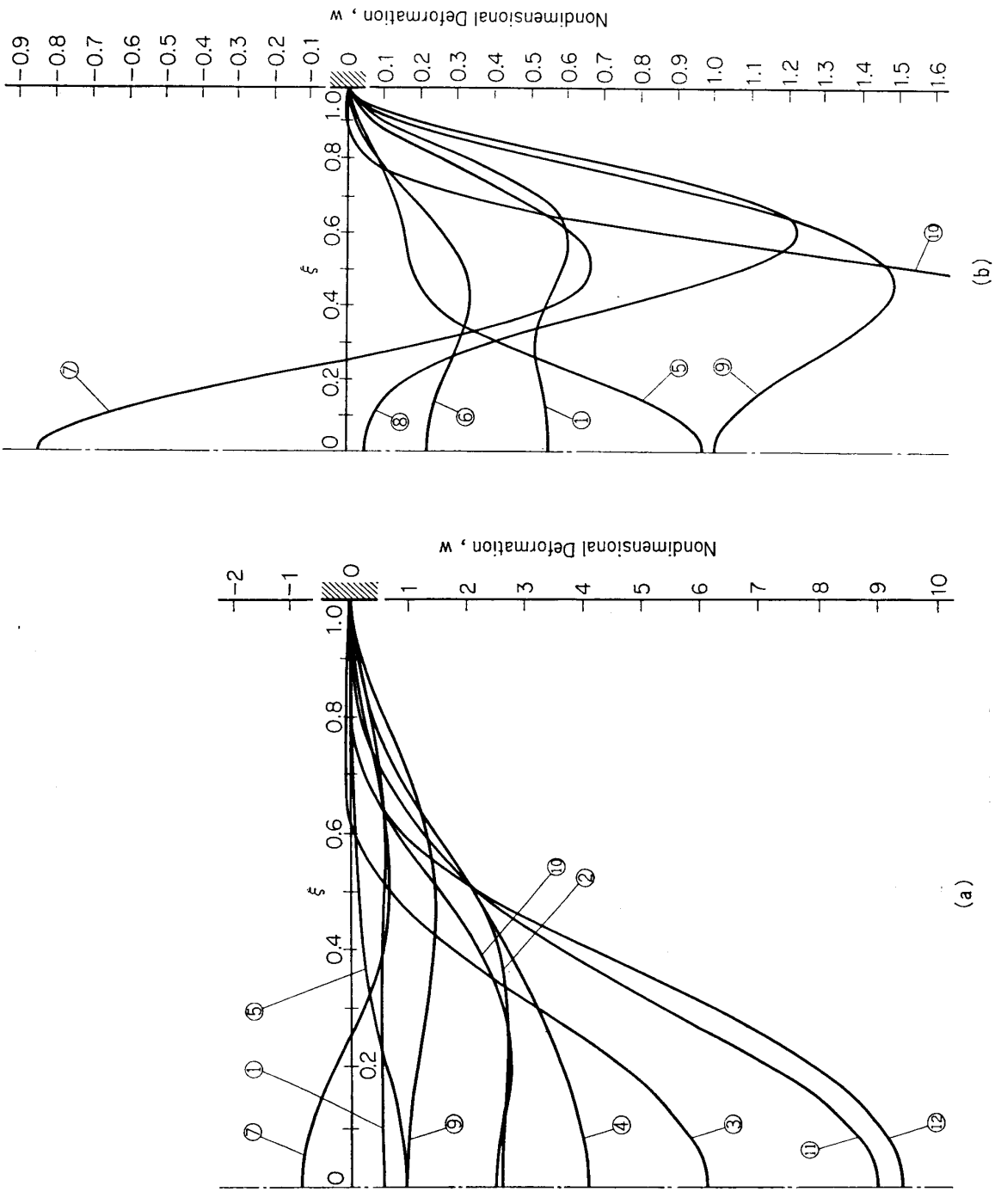


FIG. 21. Motion of an elastic shell; step loading, $p=0.470$, $\lambda=5.0$.

This document is provided by JAXA.

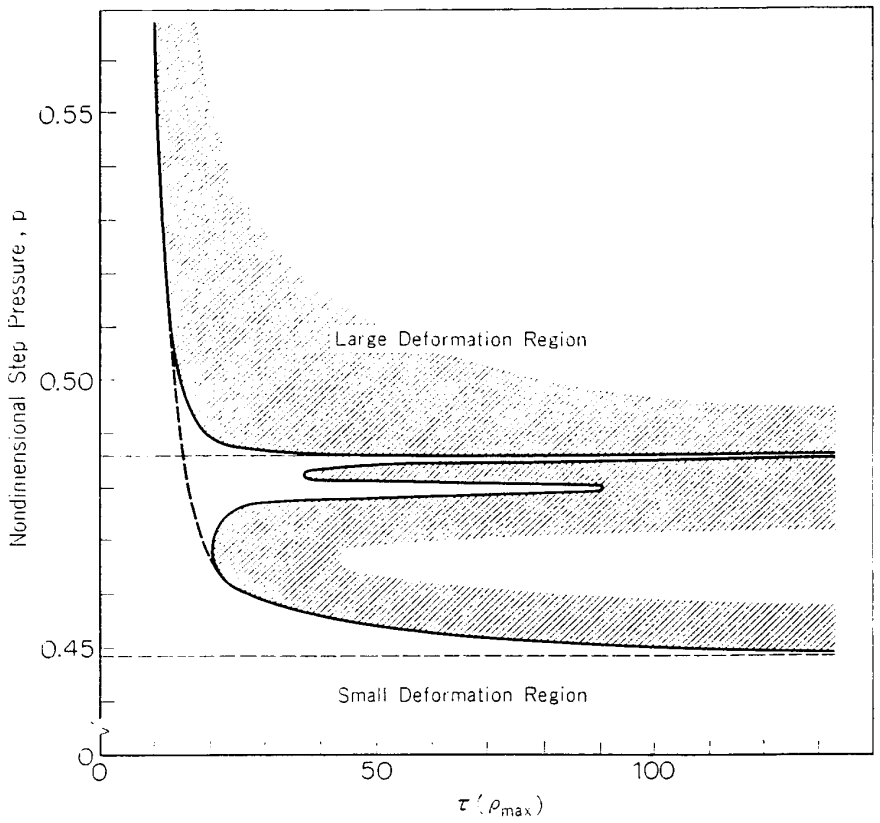


FIG. 22. Degree of ease in generating large deformation; step loading, $\lambda=5.0$, $\tau_2=\infty$.

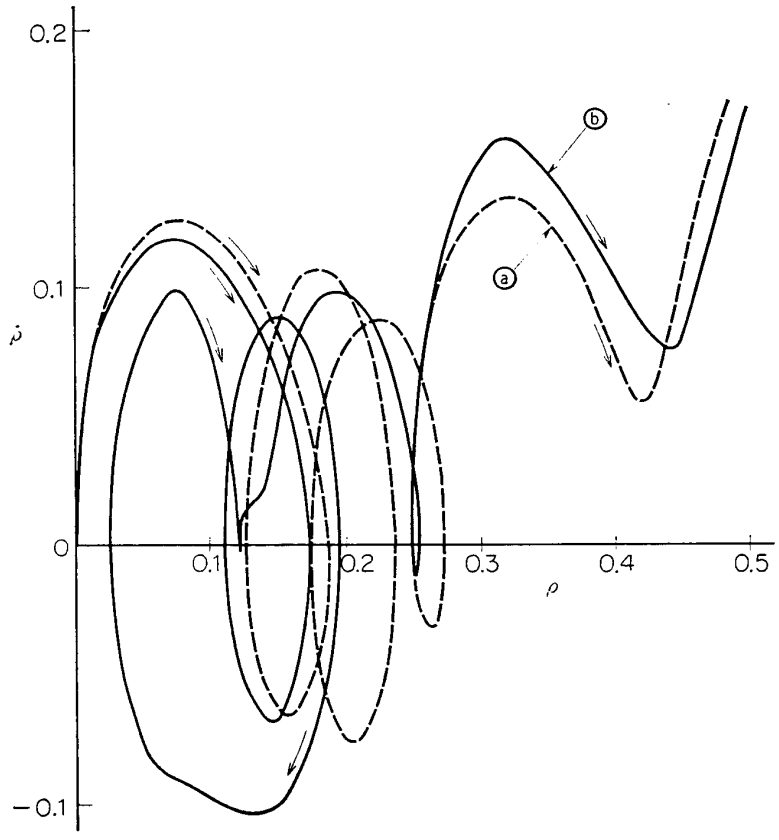


FIG. 23. Behavior of an elastic shell, step loading, $\lambda=5.0$.
ⓐ : $p=0.495$, ⓑ : $p=0.470$.

This document is provided by JAXA.

effect of damping is very large. Figure 23 shows the behavior of an elastic shell subjected to step pressures. As stated in 3.2. 2), the motion of viscoelastic shells is substantially the same only if pressure loads belong to the same deformation region, otherwise the motion is not always the same even when loads are nearly equal with one another. It can be seen in Fig. 23 that the remark mentioned above holds good in the motion of elastic shells.

This document is provided by JAXA.